

A Review of $\mu \rightarrow eee$, $\mu \rightarrow e\gamma$ and $\mu N \rightarrow eN$ Conversion

Ann-Kathrin Perrevoort^{a,*} on behalf of the Mu3e Collaboration

^a*Karlsruhe Institute of Technology, Institute of Experimental Particle Physics,
Hermann-von-Helmholtz-Platz 1, Eggenstein-Leopoldshafen, Germany*

E-mail: ann-kathrin.perrevoort@kit.edu

The observation of lepton flavour violation (LFV) in interactions involving charged leptons would be an unambiguous sign of physics beyond the Standard Model of particle physics. Given that muons can be produced at high intensities, searches for LFV with muons are particularly sensitive. In a global initiative, ongoing and upcoming experiments are aiming to discover physics beyond the Standard Model in the three golden muon LFV channels: $\mu \rightarrow e\gamma$, $\mu \rightarrow eee$ and μ -to- e conversion on nuclei. With innovative detector concepts and new muon beam lines, these experiments will be able to investigate muon LFV in the coming years with sensitivities improved by up to four orders of magnitude compared to past searches.

The current status of muon LFV searches is discussed and the ongoing MEG II and DeeMe experiments as well as the upcoming Mu2e, COMET and Mu3e experiments are presented.

*21st Conference on Flavor Physics and CP Violation (FPCP 2023)
29 May - 2 June 2023
Lyon, France*

*Speaker

1. Searches for Charged Lepton Flavour Violation with Muons

In the original formulation of the Standard Model (SM) of particle physics, lepton flavour is a conserved quantity, however, only due to an accidental symmetry. Hence, lepton flavour violation (LFV) is a common signature in numerous models of physics beyond the SM (BSM) [1]. Moreover, with the observation of neutrino oscillations it became evident that LFV processes in the neutral lepton sector occur in nature [2–4].

LFV processes in the charged lepton sector, however, have eluded observation so far. If mediated solely via neutrino mixing, charged LFV (cLFV) interactions would be suppressed to tens of orders of magnitude below the sensitivity of current and near future experiments. For the cLFV process $\mu \rightarrow e\gamma$, for example, branching ratios \mathcal{B} below 10^{-54} are predicted [5–7]. Consequently, the observation of cLFV would be an unambiguous sign of physics beyond the SM and beyond neutrino mixing.

There is a wide range of cLFV searches performed e.g. at general purpose and B -physics experiments at colliders as well as specialised kaon and muon physics experiments.

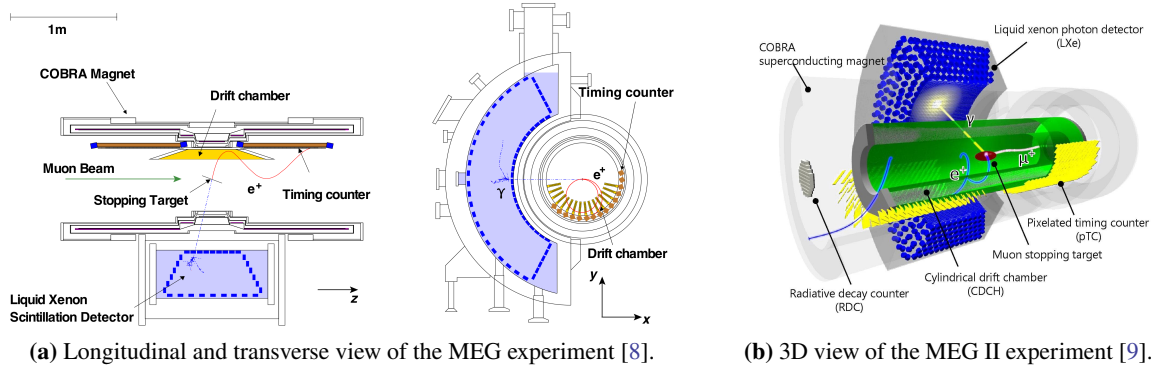
Among all types of cLFV searches, searches for μ -to- e transitions yield the strongest limits today. This is because muons can be effectively produced at high rates and decay to comparably clean final states which include only electrons, neutrinos and photons. Typically, dedicated experiments are operated at high-intensity muon sources which perform background-free searches for a selected μ -to- e LFV channel. These experiments have to meet not only the demands with regard to precision for an effective background suppression, but also have to cope with challenges arising from high muon decay rates in terms of data processing and background from accidental combinations. In addition, the muons are typically stopped in these experiments which results in decay electrons with momenta of $\mathcal{O}(10\text{ MeV})$ for which the momentum resolution is significantly deteriorated by multiple Coulomb scattering. The experiments therefore rely on detectors with minimised material amount in the active detector volume.

There is a global initiative to push the sensitivity of the so-called three golden channels $\mu^+ \rightarrow e^+\gamma$, $\mu^+ \rightarrow e^+e^-e^+$ and μ -to- e conversion on nuclei $\mu^-N \rightarrow e^-N$ by orders of magnitude in the coming years: the ongoing MEG II and DeeMe experiments as well as the upcoming COMET, Mu2e and Mu3e experiments. These experiments are presented in the following. In addition, the complementarity of the three golden channels as well as further options for BSM searches at muon cLFV experiments are discussed.

2. Searches for $\mu \rightarrow e\gamma$

The latest and currently most stringent limits on cLFV processes have been set by the MEG collaboration on the decay $\mu^+ \rightarrow e^+\gamma$ [8].

In the rest frame of the decaying muon, the signature of the signal decay is a mono-energetic positron and photon emitted back-to-back with an energy of half the muon rest mass. Background events stem from the radiative muon decay $\mu^+ \rightarrow e^+\gamma\bar{\nu}_\mu\nu_e$ in which the neutrinos are not detected, as well as from accidental coincidences of positrons and photons from different origins such as SM muon decays, Bremsstrahlung or positron annihilation. The first type of background is suppressed by precise measurements of the energy and direction of the positron and photon, and the latter type



(a) Longitudinal and transverse view of the MEG experiment [8].

(b) 3D view of the MEG II experiment [9].

Figure 1: Schematics of the MEG and MEG II experiments searching for $\mu \rightarrow e\gamma$ [8, 9].

by an accurate measurement of their relative timing as well as by operating with a continuous muon beam.

The MEG experiment is depicted in Fig. 1a. The experiment was operated from 2009 to 2013 at the $\pi E5$ channel at the Paul Scherrer Institute (PSI). The incoming continuous μ^+ beam is stopped on a slanted target in the centre of the detector at a stopping rate of $3 \times 10^7 \mu/s$. The trajectory and momentum of positrons is measured with a low-material drift chamber system placed in the COntant Bending RAdius magnet with a gradient field between 1.27 T to 0.49 T. The COBRA magnet has the advantage that the bending radius of the e^+ trajectory depends only weakly on the emission angle and that e^+ are quickly swept out of the detector even at low longitudinal momenta. An additional timing counter built from scintillating bars with photo-multiplier (PMT) readout is installed for precise measurements of the impact time and position of e^+ . The energy and timing of the photon is measured with a Liquid Xenon scintillation detector which is read out with PMTs. The direction of the photon is inferred from the interaction vertex in the LXe and the reconstructed intersection point of the trajectory of a matching positron with the target surface. The data acquisition system is triggered by information from the LXe and timing counter detectors on the photon energy and the relative direction and timing of the positron and photon.

The MEG collaboration has performed a blinded, maximum likelihood analysis on a data set of $7.5 \times 10^{14} \mu^+$ decays. As observables, the positron and photon energy E_e and E_γ , as well as the relative time $t_{e\gamma}$ and the relative azimuthal and polar angles $\theta_{e\gamma}$ and $\phi_{e\gamma}$ of the positron and photon were used to distinguish signal from background events. Event distributions are shown in Fig. 2. No significant excess with respect to the expected background was found and an upper limit on the branching ratio of $\mu^+ \rightarrow e^+\gamma$ was set at $\mathcal{B}(\mu^+ \rightarrow e^+\gamma) < 4.2 \times 10^{-13}$ at 90 % confidence level (CL) [8].

The MEG experiment underwent a substantial upgrade—MEG II—in order to boost the sensitivity of the $\mu^+ \rightarrow e^+\gamma$ search by increasing the rate capability and by improving the resolution of the detector (see Fig. 1b).

The drift chamber has been replaced by a single-volume, cylindrical drift chamber with high wire density and the timing counter by a pixelated timing counter built from scintillating tiles with Silicon Photon Multiplier (SiPM) readout. The PMTs on the entrance surface of the LXe detector were replaced by SiPMs for higher granularity. In addition, a new detector, the radiative decay counter,

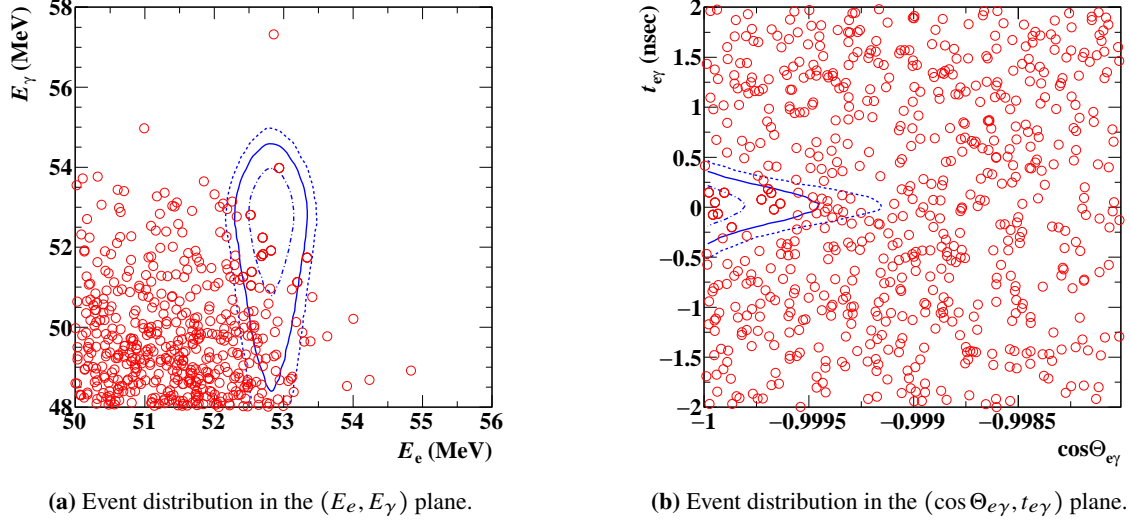


Figure 2: Distributions of observed events (red circles) and contours (1σ , 1.64σ , 2σ) of the signal probability density function (blue dashed-dotted, solid and dotted lines). $\Theta_{e\gamma}$ denotes the relative stereo angle of the positron and photon [8].

was installed downstream of the target in order to veto positrons from background processes. The radiative decay counter consists of scintillating crystals and plastic scintillators for both a precise energy and timing measurement. In this way, MEG II is capable to operate at stopping rates of $7 \times 10^7 \mu/s$ making full use of the muon beam rates available at PSI.

The MEG II experiment is taking physics data since 2021. It is expected to achieve a sensitivity to $\mathcal{B}(\mu^+ \rightarrow e^+\gamma)$ down to 6×10^{-14} at 90% CL [9].

3. Searches for $\mu \rightarrow eee$

Unlike the other golden muon LFV channels, the $\mu^+ \rightarrow e^+e^-e^+$ decay is not characterised by mono-energetic particles in the final state. Background stems on the one hand from the SM $\mu^+ \rightarrow e^+e^-e^+\bar{\nu}_\mu\nu_e$ decay which can be distinguished from signal decays only by the missing momentum from the undetected neutrinos. On the other hand, background events are generated by accidental combinations of electrons and positrons from various origins such as the dominating $\mu^+ \rightarrow e^+\bar{\nu}_\mu\nu_e$ decay, Bhabha scattering and photon conversion as well as from misreconstruction. The suppression of the first type of background requires an excellent momentum resolution in the tracking of electrons and positrons, and the suppression of the latter type accurate vertex reconstruction and timing measurement as well as a low material detector operated at a continuous muon beam.

Current limits on $\mu^+ \rightarrow e^+e^-e^+$ stem from the SINDRUM experiment which operated at PSI [10]. The SINDRUM experiment studied μ^+ decays at rest with a spectrometer built from concentric multiwire proportional chambers (MWPC) and a hodoscope made of scintillation counters placed in a 0.33 T solenoidal field. The collaboration found no events in the signal-sensitive region and set an upper limit on the branching ratio at $\mathcal{B}(\mu^+ \rightarrow e^+e^-e^+) < 1.0 \times 10^{-12}$ at 90% CL.

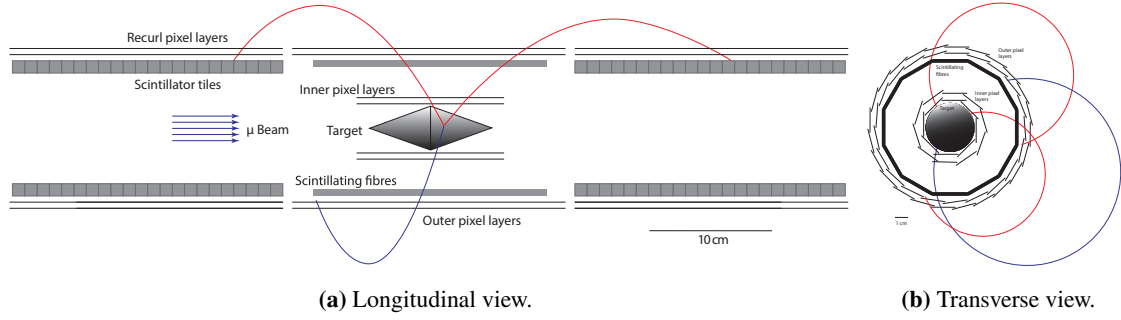


Figure 3: Schematic of the Mu3e detector in phase I [11]. The recurl stations are placed upstream and downstream of the central detector station. A $\mu^+ \rightarrow e^+e^-e^+$ signal decay is shown with positron trajectories in red and the electron trajectory in blue.

More than three decades later, the upcoming Mu3e experiment aims to repeat the search for $\mu^+ \rightarrow e^+e^-e^+$ with a sensitivity improved by four orders of magnitude compared to SINDRUM. The Mu3e experiment will be conducted in two phases. The phase I experiment is depicted in Fig. 3. The incoming, continuous μ^+ beam is stopped on a hollow, double-cone target in the centre of the experiment at a stopping rate of $10^8 \mu/s$. The detector is a low-material tracking detector built from novel, ultra-thin Silicon pixel sensors in High Voltage Monolithic Active Pixel Sensor technology [12] for precise tracking of electrons and positrons. The detector is placed in a 1 T solenoidal magnetic field with a magnet bore large enough to enable the electrons and positrons to return—or *recurl*—to the detector and be measured again. For recurling particles which have performed a half turn in-between measurements, scattering effects that deteriorate the momentum resolution cancel to first order. The detector geometry is therefore optimised for a high acceptance of recurling particles by installing recurl stations upstream and downstream of the central detector station. Additional scintillating detectors, i.e. scintillating fibres in the central station and scintillating tiles in the recurl stations, are installed for accurate timing measurements. The Mu3e experiment operates without a traditional hardware trigger. Instead, all sub-detectors continuously stream data to the event filter farm where online track reconstruction and vertex finding are performed on Graphics Processing Units. Events with $\mu^+ \rightarrow e^+e^-e^+$ candidates are selected and stored for elaborate offline reconstruction at optimum resolution and analysis. Background events will be suppressed by selections on the relative timing of the electron and positrons, the quality and position of the reconstructed vertex and kinematic observables such as the invariant mass. A distribution of simulated signal and background events from $10^{15} \mu^+$ decays is shown in Fig. 4a. The phase I Mu3e experiment has an expected sensitivity on $\mathcal{B}(\mu^+ \rightarrow e^+e^-e^+)$ of a few 10^{-15} at 90 % CL depending on the running time (see Fig. 4b). The Mu3e phase I experiment is currently under construction. First physics data runs are planned in 2025.

The Mu3e phase II experiment will be operated at muon stopping rates of $2 \times 10^9 \mu/s$ at the upcoming High-Intensity Muon Beams (HIMB) project at PSI [13]. Paired with an increased acceptance for recurling tracks and improved vertex and timing resolution, sensitivities of 10^{-16} at 90 % CL are expected. The optimum design and detector technologies are currently under investigation.

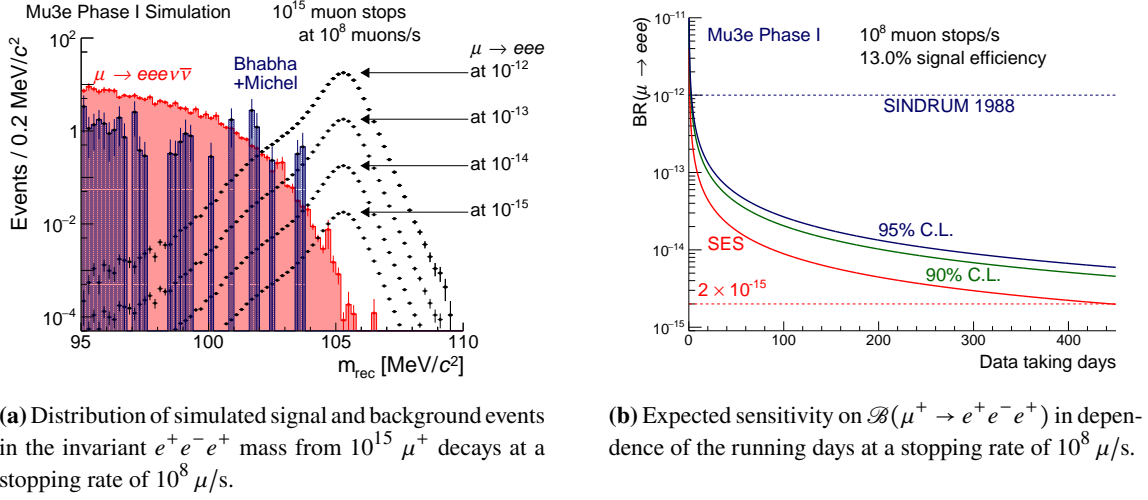


Figure 4: Simulated performance of the Mu3e experiment in phase I [11].

4. Searches for $\mu N \rightarrow eN$

Another channel to search for LFV with muons are μ -to- e conversions in muonic atoms: $\mu^-N \rightarrow e^-N$.

The measurement principle is shown in Fig. 5a. As in the previously discussed experiments, the μ^- beam is produced from a proton beam hitting a production target and the decay of the resulting pions and other hadrons to muons. The muons are then stopped on a stopping target where muonic atoms are formed. The $\mu^-N \rightarrow e^-N$ decay is characterised by a mono-energetic electron which energy is determined by the muon rest mass, the atomic binding energy of the muon and the atomic recoil energy.

Background stems from muon decays in orbit $\mu^-N \rightarrow e^- \nu_\mu \bar{\nu}_e N$ or can be beam-induced for example from pions, electrons and anti-protons as well as muon decays in flight. In addition, cosmic rays can generate background events via decay, scattering or interactions with material in the experiment. The first type of background is suppressed by an excellent energy or momentum measurement while for the last one dedicated cosmic ray vetoes are installed. Beam-induced background decays faster than muonic atoms and can therefore be reduced by the usage of a pulsed proton beam and by starting data recording only several 100 ns after the proton pulse (see Fig. 5b). Target materials are typically chosen with the requirement of long lifetimes for the muonic atom.

The current most stringent limits on $\mu^-N \rightarrow e^-N$ stem from the SINDRUM II experiment at PSI. The SINDRUM II experiment used a Gold foil as stopping target and measured the electron trajectories with a combination of a drift chamber and a scintillator and Cerenkov hodoscope placed in a solenoidal magnetic field. Proton pulses were generated every 19.75 ns. SINDRUM II collected a total of $4.37(32) \times 10^{13}$ μ^- stopped on target. The momentum distributions of the observed events are shown in Fig. 6. No significant excess above the expected background was found and an upper limit on the conversion rate was set at $\mathcal{R}(\mu^- \text{Au} \rightarrow e^- \text{Au}) < 7.0 \times 10^{-13}$ at 90% CL [14].

Three experiments will repeat the search for $\mu^-N \rightarrow e^-N$ in the near future: DeeMe [17] and COMET [18] at J-PARC and Mu2e [19] at Fermilab.

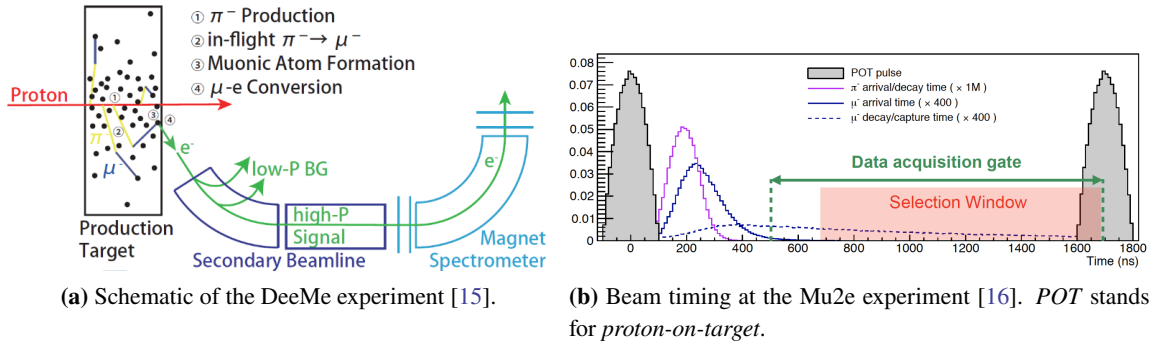


Figure 5: Principle of $\mu^- N \rightarrow e^- N$ searches.

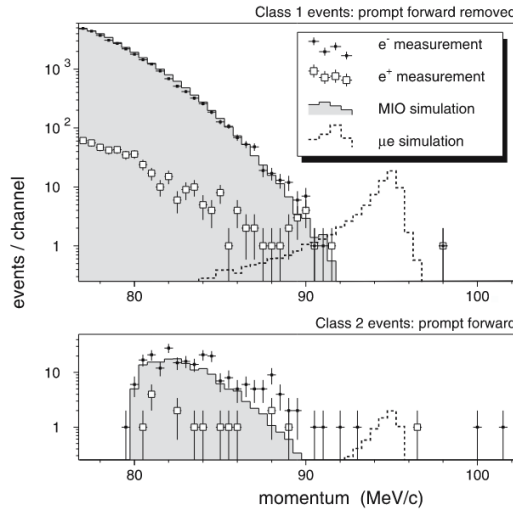


Figure 6: Distributions of the momentum of observed electrons and positrons as well as signal and background predictions in the SINDRUM II experiment. Beam-induced background is correlated with the proton pulse on the production target and thus appears promptly with the arrival of muons on the stopping target and tends to be forward-directed. *MIO* stands for *muon decay in orbit*. [14]

The DeeMe experiment will search for μ -to- e conversion on Carbon. A schematic of the experiment is shown in Fig. 5a. The 3 GeV Rapid Cycling Synchrotron delivers proton double pulses at a frequency of 25 Hz allowing to have 10 μ s long data taking intervals starting around 300 ns after the second pulse. The Carbon target serves as both muon production and muon stopping target. With a secondary beamline, electrons from signal processes are separated from electrons from background processes which tend to have lower momenta. Positively charged particles are removed, as well. The electrons momenta are then measured in a magnet spectrometer consisting of a 0.4 T dipole magnet bending the beam by 70° and two times two thin MWPCs upstream and downstream of the magnet. The high voltage at the MWPCs is switched to a high gas gain mode only during the data acquisition windows for detector protection in intervals of high prompt background. The DeeMe collaboration has performed commissioning runs and is getting ready to take physics data. A sensitivity to the conversion rate on Carbon of $\mathcal{R}_{\mu e}(\mu^- C \rightarrow e^- C) \lesssim 2 \times 10^{-13}$ at 90% CL is expected.

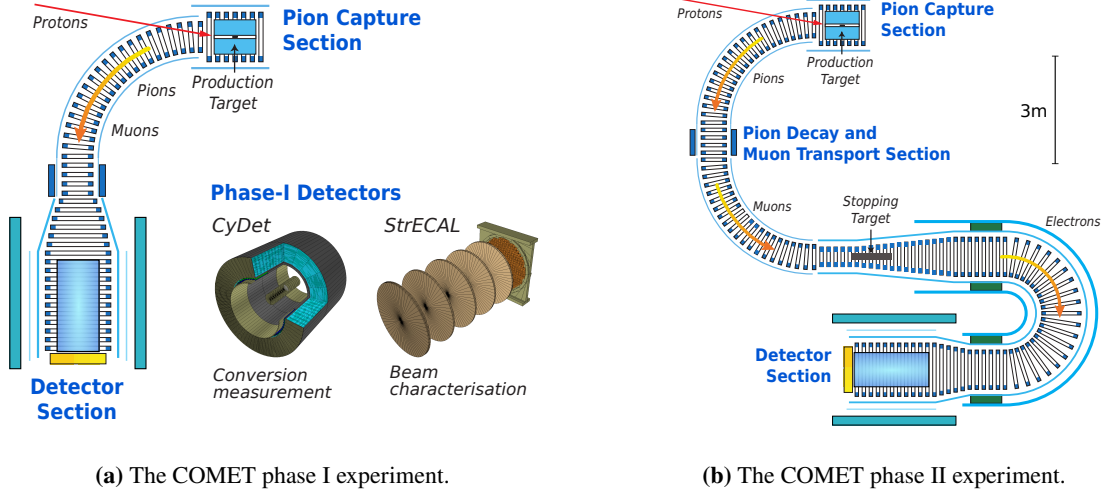


Figure 7: Schematic of the COMET experiment in phase I and II [18, 20].

The second upcoming experiment at J-PARC is the two-staged COherent Muon to Electron Transition experiment. COMET searches for μ -to- e conversion on Aluminum. A schematic of the experiment in its two stages is shown in Fig. 7.

In contrast to DeeMe, the muon production and muon stopping target are separated which allows for a more efficient suppression of beam-induced background. Muons are produced by directing a pulsed proton beam with bunch intervals of around $1.17 \mu\text{s}$ on a graphite target. In phase I, the stopping target is separated from the production target by a 90° transport solenoid (see Fig. 7a). The stopping target is built from aluminum discs located inside the detector section and delivers stopping rates of $1.2 \times 10^9 \mu/\text{s}$. It is surrounded by the Cylindrical Detector (CyDet) consisting of a cylindrical drift chamber and a trigger hodoscope built from two layers of plastic scintillators. The additional StrECAL detector—a combination of a straw tube tracker and an electromagnetic calorimeter built from LYSO crystals read out by avalanche photodiodes—performs direct beam measurements. The StrECAL is moreover a prototype for the phase II detector. The Cosmic Ray Veto is built from scintillators as well as glass Resistive Plate Chambers.

The COMET phase I experiment is currently under construction and is planned to commence data taking in 2024/2025. A sensitivity of $\mathcal{R}_{\mu e}(\mu^- \text{Al} \rightarrow e^- \text{Al}) \lesssim 7.0 \times 10^{-15}$ at 90% CL is expected.

In phase II, the production target will be replaced by a tungsten target. Combined with improvements on the proton beam and capture solenoid, a muon production increased by a factor of twenty is expected. The muon transport solenoid will be extended to a full 180° turn. The muon stopping target will be separated from the detector section by a C-shaped electron spectrometer and the muon stopping efficiency will be increased. The COMET II experiment will be sensitive to $\mathcal{R}_{\mu e}(\mu^- \text{Al} \rightarrow e^- \text{Al}) < 3.2 \times 10^{-17}$ at 90% CL.

As a successor of COMET, there is another upgrade under investigation at J-PARC, the Phase Rotated Intense Slow Muon source PRISM which features a muon storage ring and the PRISM Muon to Electron conversion experiment PRIME [21]. The PRISM/PRIME project is expected to reach sensitivities on $\mathcal{R}_{\mu e}$ of 10^{-18} .

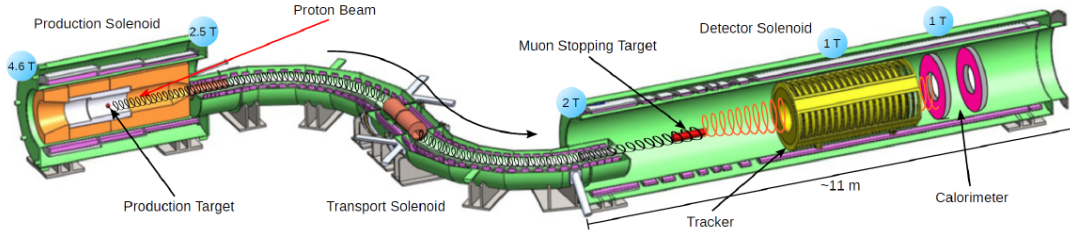


Figure 8: Schematic of the Mu2e experiment [19].

The Mu2e experiment at Fermilab also searches for $\mu^- \text{Al} \rightarrow e^- \text{Al}$ in two stages [19]. A schematic of the experiment is shown in Fig. 8.

A pulsed 8 GeV proton beam hits a tungsten muon production target with a pulse every $1.7 \mu\text{s}$. The production target is separated from the muon stopping target and detector section by an S-shaped transport solenoid. The stopping target is located in front of the tracker and calorimeter inside the detector solenoid. In phase I, muon stopping rates of $10^{10} \mu/\text{s}$ are envisaged. The tracking detector is a straw tube tracker while the calorimeter is constructed from scintillating crystals with SiPM readout. Each side of the detector solenoid hall is covered with four layers of scintillators which serve as cosmic ray veto.

The phase I experiment is currently under construction and is expected to commence data taking in 2025. It will have a sensitivity of $\mathcal{R}_{\mu e}(\mu^- \text{Al} \rightarrow e^- \text{Al}) < 6.2 \times 10^{-16}$ at 90 % CL.

The Mu2e phase II experiment will be operated at a proton beam intensity increased by a factor of ten enabled by the Proton-Improvement-Plan-II PIP-II at Fermilab. Combined with improvements on all systems, sensitivities of $\mathcal{R}_{\mu e}(\mu^- \text{Al} \rightarrow e^- \text{Al}) < 6 \times 10^{-17}$ at 90 % CL are in reach of Mu2e phase II.

5. Complementary of Muon cLFV Searches

The sensitivity of the three golden channels to different types of BSM interactions can be studied and compared by means of effective field theories (see for example [22]). As shown in Fig. 9, each channel has specific strengths and weaknesses in constraining the various interactions. Thus, the interplay of potential observations and non-observations in the muon LFV channels will allow to draw a more complete picture of favoured and disfavoured BSM models.

Furthermore, it is possible to distinguish certain effective operators directly in $\mu^- N \rightarrow e^- N$ and $\mu^+ \rightarrow e^+ e^- e^+$ searches.

In $\mu^- N \rightarrow e^- N$, the dependence of the conversion rate on the atomic number Z of the nucleus varies for the different operators (see Fig. 10). Thus, searches with different target materials can be used to narrow down the type of BSM interaction. However, the choice of suited target materials is limited as the lifetime of the muonic atom needs to be sufficiently long and as well as for technical reasons. In addition to aluminum, for example titanium, vanadium and lithium are considered.

In the case of $\mu^+ \rightarrow e^+ e^- e^+$, the kinematics of the final decay products can reveal the type of BSM interaction. In Fig. 11, Dalitz plots of the invariant mass squared of the two possible $e^+ e^-$ pairs

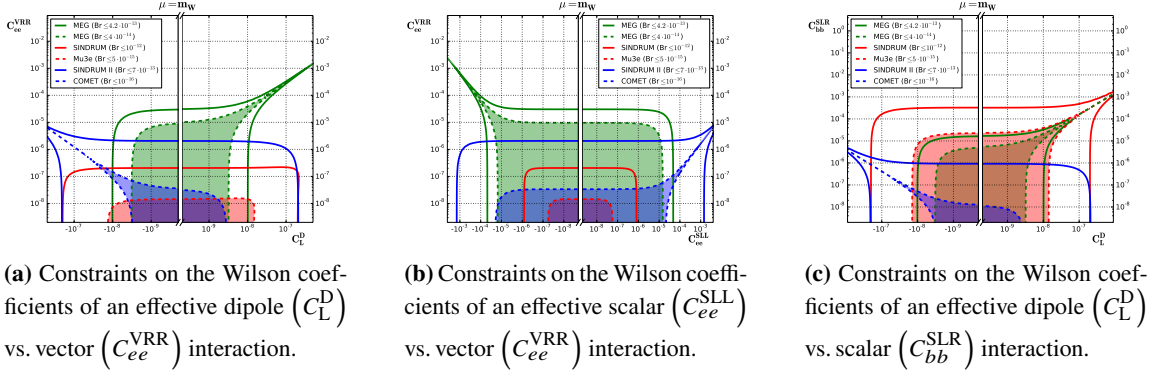


Figure 9: Observed and prospected constraints on Wilson coefficients in muon LFV effective field theories from current and future searches for $\mu^+ \rightarrow e^+ \gamma$, $\mu^+ \rightarrow e^+ e^- e^+$ and $\mu^- N \rightarrow e^- N$ [22].

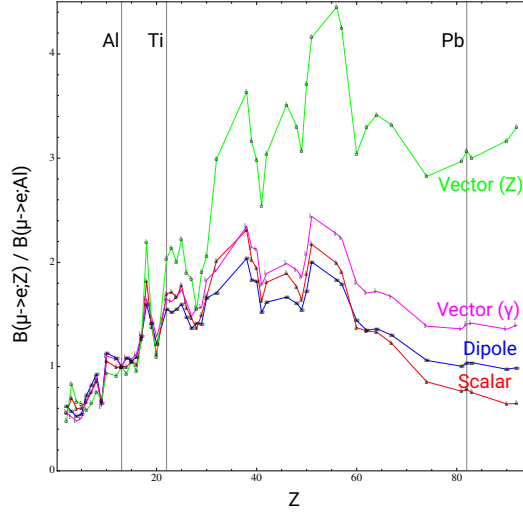


Figure 10: Dependence on the conversion rate in $\mu^- N \rightarrow e^- N$ transitions mediated via different effective interactions on the atomic number Z of the nuclei. Adapted from [23].

are shown. Different effective operators reveal characteristic distributions that allow to distinguish various BSM interactions.

6. Exotic Physics at Muon Experiments

Despite being designed to investigate one specific channel, the above mentioned experiments are not limited to a single measurement. A selection of searches that go beyond the scope are presented in the following.

The ATOMKI collaboration has reported the observation of an excess in the angular distributions of internal pair creation in the transition ${}^7\text{Li}(p, e^+ e^-){}^8\text{Be}$ [26] as well as in the transition ${}^3\text{H}(p, e^+ e^-){}^4\text{He}$ [27]. This excess would be compatible with the production and subsequent decay of a hypothetical BSM boson at a mass of around 17 MeV commonly referred to as $X(17)$.

The MEG II experiment will repeat this measurement using a p beam from a Cockcroft-Walton

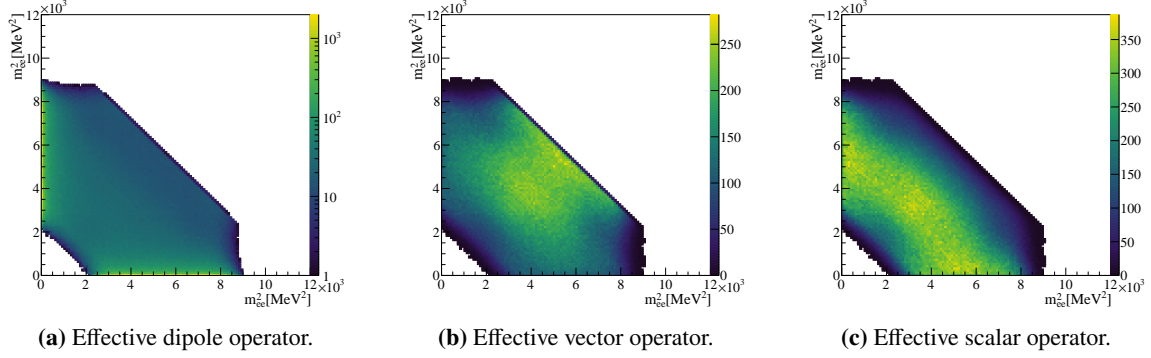


Figure 11: Dalitz plots of the invariant mass squared of e^+e^- pairs from $\mu^+ \rightarrow e^+e^-e^+$ mediated via various effective operators in the Mu3e phase I experiment [24]. The effective Lagrangian is taken from [25].

accelerator and a $\text{Li}_2\text{B}_4\text{O}_7$ target which are normally used for calibration purposes [28]. The collaboration has taken first data for this measurement.

In addition, the Mu3e collaboration will perform searches for e^+e^- resonances in $\mu^+ \rightarrow e^+e^-e^+\bar{\nu}_\mu\nu_e$ in view of searches for dark photons [24]. This search will also be sensitive to $X(17)$.

Another channel that will be investigated with the Mu3e experiment is $\mu^+ \rightarrow e^+X$ in which X is an axion-like particle from a broken flavour symmetry like a familon or majoron [29, 30] that leaves the detector unseen. For this purpose, the Mu3e data acquisition is adapted to accommodate online histogramming of track fit results such as momenta and emission angles of events with single positrons on the event filter farm. Current limits on $\mu^+ \rightarrow e^+X$ are set by Jodidio et al. at $\mathcal{B}(\mu^+ \rightarrow e^+X) < 2.6 \times 10^{-6}$ at 90 % CL for massless X [31], and by the TWIST collaboration at $\mathcal{B}(\mu^+ \rightarrow e^+X) < 9 \times 10^{-6}$ at 90 % CL on average for X with masses between 13 MeV and 80 MeV. The sensitivity of the Mu3e experiment in phase I exceeds the limits set by TWIST by two orders of magnitude in a large range of X masses (see Fig. 12) and will be further improved in phase II due to a twenty times larger number of observed muon decays and an enhanced detector performance. Searches for $\mu^+ \rightarrow e^+X$ will be also performed at MEG II [30, 32] and at the $\mu N \rightarrow eN$ experiments Mu2e and COMET [33, 34]. MEG II will further investigate the channel $\mu^+ \rightarrow e^+\gamma X$.

Furthermore, the lepton flavour and lepton number violating process $\mu^- N \rightarrow e^+ N'$ can be investigated at the muon conversion experiments Mu2e and COMET [36], however they require a better theoretical understanding of the background contribution of radiative muon capture $\mu^- N \rightarrow \nu_\mu N' \gamma$ with $\gamma \rightarrow e^+e^-$. Current upper limits are set by SINDRUM II measurements with a titanium target at $\mathcal{R}(\mu\text{Ti} \rightarrow e^+\text{Ca}) < 1.7 \times 10^{-12}$ at 90 % CL [37].

7. Summary

The observation of cLFV μ -to- e transitions would be an unambiguous sign of BSM physics. Several experiments are currently operating or under construction which will investigate these transitions with an up to four orders improved sensitivity compared to current limits: the ongoing MEG II experiment at PSI searching for $\mu^+ \rightarrow e^+\gamma$, the upcoming Mu3e experiment at PSI searching for $\mu^+ \rightarrow e^+e^-e^+$, and the ongoing DeeMe experiment and the upcoming COMET experiment at

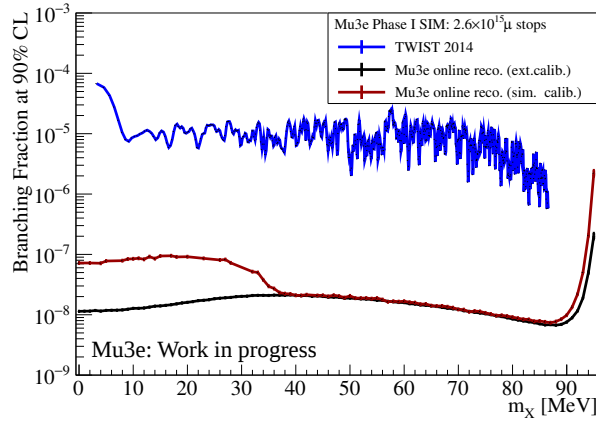


Figure 12: Sensitivity of the Mu3e phase I experiment to $\mu^+ \rightarrow e^+ X$ compared to current most stringent limits set by TWIST [24]. Two scenarios for the calibration of the momentum scale are shown: one assuming calibration using an external process (*ext. calib.*), and the other one assuming simultaneous calibration using the momentum spectrum of $\mu^+ \rightarrow e^+ \bar{\nu}_\mu \nu_e$ decays (*sim. calib.*). TWIST results by courtesy of R. Bayes [35].

J-PARC as well as the upcoming Mu2e experiment at Fermilab searching for μ -to- e conversion on nuclei $\mu^- N \rightarrow e^- N$. The complementarity of these searches allows to narrow down the type of BSM interaction in case of discovery or strongly constrain numerous BSM models in case of non-observation. In addition, further BSM signatures can be investigated by these experiments with competitive sensitivity.

References

- [1] L. Calibbi and G. Signorelli, *Charged lepton flavour violation: An experimental and theoretical introduction*, *Riv. Nuovo Cim.* **41** (2018) 71 [1709.00294].
- [2] SUPER-KAMIOKANDE collaboration, *Evidence for oscillation of atmospheric neutrinos*, *Phys. Rev. Lett.* **81** (1998) 1562 [hep-ex/9807003].
- [3] SNO collaboration, *Measurement of the rate of $\nu_e + d \rightarrow p + p + e^-$ interactions produced by ^8B solar neutrinos at the Sudbury Neutrino Observatory*, *Phys. Rev. Lett.* **87** (2001) 071301 [nucl-ex/0106015].
- [4] KAMLAND COLLABORATION collaboration, *First results from KamLAND: Evidence for reactor anti- neutrino disappearance*, *Phys. Rev. Lett.* **90** (2003) 021802 [hep-ex/0212021].
- [5] S.T. Petcov, *The Processes $\mu \rightarrow e + \gamma$, $\mu \rightarrow e + \bar{e}$, $\nu' \rightarrow \nu + \gamma$ in the Weinberg-Salam Model with Neutrino Mixing*, *Sov. J. Nucl. Phys.* **25** (1977) 340.
- [6] S.M. Bilenky, S.T. Petcov and B. Pontecorvo, *Lepton Mixing, $\mu \rightarrow e + \gamma$ Decay and Neutrino Oscillations*, *Phys. Lett. B* **67** (1977) 309.
- [7] A. de Gouvea and P. Vogel, *Lepton Flavor and Number Conservation, and Physics Beyond the Standard Model*, *Prog.Part.Nucl.Phys.* **71** (2013) 75 [1303.4097].

- [8] MEG collaboration, *Search for the lepton flavour violating decay $\mu^+ \rightarrow e^+ \gamma$ with the full dataset of the MEG experiment*, *Eur. Phys. J. C* **76** (2016) 434 [1605.05081].
- [9] MEG II collaboration, *The design of the MEG II experiment*, *Eur. Phys. J. C* **78** (2018) 380 [1801.04688].
- [10] SINDRUM collaboration, *Search for the decay $\mu^+ \rightarrow e^+ e^+ e^-$* , *Nucl. Phys. B* **299** (1988) 1.
- [11] Mu3E collaboration, *Technical design of the phase I Mu3e experiment*, *Nucl. Instrum. Meth. A* **1014** (2021) 165679 [2009.11690].
- [12] I. Peric, *A novel monolithic pixelated particle detector implemented in high-voltage CMOS technology*, *Nucl. Instrum. Meth. A* **582** (2007) 876.
- [13] M. Aiba et al., *Science case for the new High-Intensity Muon Beams HIMB at PSI*, 2111.05788.
- [14] SINDRUM II collaboration, *A Search for muon to electron conversion in muonic gold*, *Eur. Phys. J. C* **47** (2006) 337.
- [15] Aoki Group, Department of Physics, Osaka University, *DeeMe experiment*, <https://www-epp.phys.sci.osaka-u.ac.jp/deeme/>, 2023.
- [16] R.H. Bernstein, *The Mu2e experiment*, *Frontiers in Physics* **7** (2019) .
- [17] H. Natori (DeeMe collaboration), *DeeMe experiment - An experimental search for a mu-e conversion reaction at J-PARC MLF*, *Nucl. Phys. B Proc. Suppl.* **248-250** (2014) 52.
- [18] COMET collaboration, *COMET phase-I technical design report*, *PTEP* **2020** (2020) 033C01 [1812.09018].
- [19] Mu2E collaboration, *Mu2e technical design report*, 1501.05241.
- [20] B.E. Krikler (COMET collaboration), *An Overview of the COMET Experiment and its Recent Progress*, in *17th International Workshop on Neutrino Factories and Future Neutrino Facilities*, 12, 2015 [1512.08564].
- [21] Y. Kuno, *PRISM/PRIME*, *Nuclear Physics B - Proceedings Supplements* **149** (2005) 376.
- [22] A. Crivellin, S. Davidson, G.M. Pruna and A. Signer, *Renormalisation-group improved analysis of $\mu \rightarrow e$ processes in a systematic effective-field-theory approach*, *JHEP* **05** (2017) 117 [1702.03020].
- [23] V. Cirigliano, R. Kitano, Y. Okada and P. Tuzon, *On the model discriminating power of $\mu \rightarrow e$ conversion in nuclei*, *Phys. Rev. D* **80** (2009) 013002 [0904.0957].
- [24] A.-K. Perrevoort (Mu3e collaboration), *The rare and forbidden: Testing physics beyond the standard model with Mu3e*, *SciPost Phys. Proc.* **1** (2019) 052 [1812.00741].

- [25] Y. Kuno and Y. Okada, *Muon decay and physics beyond the Standard Model*, *Rev. Mod. Phys.* **73** (2001) 151 [[hep-ph/9909265](#)].
- [26] A.J. Krasznahorkay et al., *Observation of anomalous internal pair creation in Be8 : A possible indication of a light, neutral boson*, *Phys. Rev. Lett.* **116** (2016) 042501 [[1504.01527](#)].
- [27] A.J. Krasznahorkay et al., *A new anomaly observed in ^4He supporting the existence of the hypothetical X17 particle*, *J. Phys. Conf. Ser.* **1643** (2020) 012001.
- [28] D.S.M. Alves et al., *Shedding light on X17: community report*, *Eur. Phys. J. C* **83** (2023) 230.
- [29] F. Wilczek, *Axions and family symmetry breaking*, *Phys. Rev. Lett.* **49** (1982) 1549.
- [30] L. Calibbi, D. Redigolo, R. Ziegler and J. Zupan, *Looking forward to lepton-flavor-violating ALPs*, *JHEP* **09** (2021) 173 [[2006.04795](#)].
- [31] A. Jodidio et al., *Search for right-handed currents in muon decay*, *Phys. Rev. D* **34** (1986) 1967.
- [32] Y. Jho, S. Knapen and D. Redigolo, *Lepton-flavor violating axions at MEG II*, *JHEP* **10** (2022) 029 [[2203.11222](#)].
- [33] Y. Kuno, C. Wu and T. Xing, *Letter of interest: Possibility of search for bound $\mu^- \rightarrow e^- a$ decay*, in *2022 Snowmass Summer Study*, 2022, https://www.snowmass21.org/docs/files/summaries/RF/SNOWMASS21-RF5_RF0_C_Wu-120.pdf.
- [34] T. Xing, C. Wu, H. Miao, H.-B. Li, W. Li, Y. Yuan et al., *Search for Majoron at the COMET experiment**, *Chin. Phys. C* **47** (2023) 013108 [[2209.12802](#)].
- [35] TWIST collaboration, *Search for two body muon decay signals*, *Phys. Rev. D* **91** (2015) 052020 [[1409.0638](#)].
- [36] M. Lee and M. MacKenzie, *Muon to Positron Conversion*, *Universe* **8** (2022) 227 [[2110.07093](#)].
- [37] SINDRUM II collaboration, *Improved limit on the branching ratio of $\mu^- \rightarrow e^+$ conversion on titanium*, *Phys. Lett. B* **422** (1998) 334.

Acknowledgments

The author's work is funded by the Federal Ministry of Education and Research (BMBF) and the Baden-Württemberg Ministry of Science as part of the Excellence Strategy of the German Federal and State Governments.